Quantitative lithium mapping of lithium-ion battery cathode using laser-induced breakdown spectroscopy

doi: 10.1016/j.jpowsour.2018.07.088

Quantitative lithium mapping of lithium-ion battery cathode using laser-induced breakdown spectroscopy

Susumu Imashuku[a], Hiroyuki Taguchi[a], Toru Kawamata[b], Shun Fujieda[b], Shunsuke Kashiwakura[a], Shigeru Suzuki[b], Kazuaki Wagatsuma[a]

[a]Institute for Materials Research, Tohoku University, 2-1-1 Katahira, Aoba-ku, Sendai 980-8577, Japan
[b]Institute of Multidisciplinary Research for Advanced Materials, Tohoku University, Katahira, Aoba-ku, Sendai 980-8577, Japan

Corresponding author: Susumu Imashuku
E-mail: susumu.imashuku@imr.tohoku.ac.jp
TEL: +81-22-215-2132
FAX: +81-22-215-2131

ABSTRACT

A method to obtain the quantitative lithium distribution of a lithium-ion battery cathode using laser-induced breakdown spectroscopy (LIBS) measurements is proposed. We perform LIBS measurements in a reduced argon atmosphere of 1000 Pa and use a calibration curve obtained by measuring the emission intensities at 610.4 nm of standard samples, whose atomic ratios of lithium to cobalt are 0, 0.10, 0.30, 0.51, 0.62, 0.80, and 0.99. The lithium distributions of cycled cathodes, which contain $LiCoO_2$ as an active material, obtained by this method are relatively consistent with the Co(III) distributions obtained by X-ray absorption spectroscopy (XAS). XAS is the conventional method to quantitatively display the reaction distribution of a cathode material used in a lithium-ion battery. Additionally, LIBS can detect the precipitating decomposition products of the electrolyte, LiF, on the cathode. However, the precision of the lithium ratio using LIBS is not as good as that achieved for the Co(III) ratio obtained using XAS. Therefore, LIBS is suitable to obtain a quantitative or semi-quantitative lithium distribution of a cathode of a lithium-ion battery and to detect the decomposition product of the electrolyte using laboratory-scale measurements.

Keywords: Lithium distribution, Laser-induced breakdown spectroscopy, Cathode, Lithium fluoride, X-ray absorption spectroscopy

1. Introduction

Lithium-ion batteries are used worldwide in portable devices such as laptop computers, cell-phones, and digital cameras. They have also recently been applied to large-scale devices like electric vehicles and stationary electric energy storage systems. A higher charge–discharge rate capacity is demanded for lithium-ion batteries to be more widely applicable in large-scale devices [1-4] because they require a high power output and a rapid charge–discharge cycle. However, a non-uniform reaction distribution on the cathodes hinders this demand from being satisfied [4-12]. Thus, a major challenge is to prevent the non-uniform reaction distribution of the cathodes at high charge–discharge rates. The establishment of an analytical method to quantitatively visualize the reaction distribution of the cathode has played an important role in overcoming this challenge. Several techniques have been proposed for the visualization of the reaction distribution of the cathode: Raman spectroscopy [13,14], X-ray absorption spectroscopy (XAS) [4,6-9,15-23], X-ray diffraction (XRD) [5,24], laser-induced breakdown spectrometry (LIBS) [10,25-29], X-ray tomography [30], atomic force microscopy (AFM) [31], particle induced γ-ray emission (PIGE) [32], neutron depth profiling [33], and electron forward scattering diffraction (EFSD) [34]. Among these techniques, LIBS is one of the most straightforward analytical methods to visualize the reaction distribution of the cathode. LIBS is an analytical technique to acquire an optical spectrum emitted from atoms evaporated from a sample as a result of the irradiation of a pulsed laser with a high power density. The light emission occurs during the deexcitation of the evaporated atoms in a plasma formed by the pulsed laser irradiation. LIBS can be performed in a laboratory (does not require large-scale facilities such as a synchrotron radiation facility) without any pretreatment of the sample; however, LIBS is a destructive analysis and is difficult to carry out *in situ*. Additionally, LIBS measurements are not restricted by the shape and thickness of the sample. LIBS can directly detect signals from

lithium, that is, light associated with the deexcitation of lithium atoms in a plasma produced using an intense laser pulse, unlike XAS, Raman spectroscopy, XRD, X-ray tomography, AFM, and EFSD.

Previously reported lithium distributions of cathodes measured by LIBS were qualitative [5,25-29] because the measurement samples were exposed to ambient pressure. Under the measurement conditions, light emitted from lithium atoms suffers a strong self-absorption effect, that is, the reabsorption of the emitted luminescence by atoms in their fundamental electronic levels in the plasma and located in the colder external part of the plasma [35]. As a result, the intensity of the light emitted from lithium atoms is reduced and does not linearly correspond to the lithium concentration in the cathodes, especially at high lithium concentrations [5]. Thus, it is difficult to obtain the quantitative lithium distribution by ambient pressure LIBS measurements even though standard samples are used [26-28]. Therefore, the reduction of the self-absorption effect is essential to obtain quantitative lithium distributions of the cathode by LIBS. One way to solve this problem is to carry out LIBS measurements in an argon atmosphere. Fabre et al. reported that sweeping samples with an argon flow improved the intensity of the emission lines of lithium in the LIBS measurement of geological materials containing lithium [35]. It has also been reported that the self-absorption effect was buffered under a reduced pressure [36,37].

In this paper, we establish a method to quantitatively acquire the lithium distribution of the cathode of a lithium-ion battery by performing LIBS measurements in a reduced argon atmosphere. Subsequently, we examine the advantages of this method by comparing it with XAS, which is a widely-used technique for visualizing the reaction distribution of the cathode of a lithium-ion battery. We select $LiCoO_2$ as an active material in the cathode because it is one of the most widely-used active materials in lithium-ion batteries.

2. Experimental

The experimental set-up of the LIBS system is shown in Fig. 1. The laser used in the present study was a Q-switched Nd: YAG laser (LOTIS TII, LS-2137) with a wavelength of 532 nm. The energy and duration of the pulsed laser irradiated on the samples were 20 mJ/pulse and 16–18 ns, respectively. A single pulse from the laser was shot onto the samples for each measurement point. The laser was focused on the sample surface using a plano-convex lens with a focal length of 150 mm. The light emitted from the plasma was collected, using a plano-convex lens with a focal length of 100 mm, through an optical fiber to a spectrometer system consisting of a spectrograph and an ICCD detector. We used two types of spectrometer systems for the LIBS measurement. A spectrometer system consisting of an Echelle-type spectrograph (ME5000, Andor Technology Ltd., Belfast, UK) and an ICCD detector (DH734-18F, Andor Technology Ltd., Belfast, UK) was used to determine the analytical line of lithium because the spectrometer system could collect spectra over a wide wavelength range (200–895 nm). After determining the analytical line of lithium, a spectrometer system consisting of a Czerny-Turner spectrograph (MS 7504i, SOL instruments Ltd., Minsk, Belarus) and an ICCD detector (DH334T-18F-03, Andor Technology Ltd., Belfast, UK) was used because of its high sensitivity but narrow wavelength range (13.3 nm). The gate of the ICCD detectors was triggered by the laser and the relative delay was controlled by the digital delay generator integrated in the ICCD detectors. The gate width and the relative delay were set to 20 μs and 800 ns, respectively. The samples were placed in a chamber, which enabled the atmosphere to be controlled by introducing gas and the connection of a rotary pump. The pressure inside the chamber was monitored using a Pirani gauge. The analyzed positions of the sample in the x and y directions were controlled by placing the chamber on linear transition automatic stages. The height of the samples was adjusted by rotating the sample stage connected to the chamber with a screw.

We chose $LiCoO_2$ as the active material in the cathode. Before LIBS analysis of the cathode, we first measured the emission intensities of standard samples, whose atomic ratios of lithium to cobalt (X) were 0, 0.01, 0.10, 0.30, 0.51, 0.62, 0.80, and 0.99, by LIBS to determine the analytical line of lithium and obtain a calibration curve for the quantitative analysis of lithium. The standard samples apart from $X = 0$ were prepared by a solid state reaction of lithium carbonate (Li_2CO_3) (purity: 98.0%, NACALAI TESQUE, INC.) and cobalt oxide (Co_3O_4) (purity: 99.9%, Kojundo Chemical Laboratory Co., Ltd.) powders. The raw materials were mixed at various mix ratios with an agate motor and then heated at 1173 K for 20 hours in air. The obtained powders were pressed into pellets at 500 MPa. The standard sample with $X = 0.99$ was confirmed to be a single phase of $LiCoO_2$, while the standard samples with $X = 0.01$, 0.10, 0.30, 0.51, 0.60, and 0.80 were shown to be a mixture of $LiCoO_2$ and Co_3O_4 by X-ray diffraction using the Cu-Kα line (Ultima IV, Rigaku Corporation, Tokyo, Japan). We used Co_3O_4 as the standard sample with $X = 0$. The compositions of the standard samples apart from $X = 0$ were measured by inductively coupled plasma atomic emission spectroscopy (ICP-AES) (IRIS Advantage DUO, Thermo Fisher Scientific, Inc., Waltham, Massachusetts, USA).

The cathode material was prepared by mixing $LiCoO_2$ powder (purity: 99.8%, Sigma-Aldrich), acetylene black, and polytetrafluoroethylene at a weight ratio of 14:5:1. The mixture was stretched into a sheet with a thickness of approximately 100 μm using an agate mortar. The cathode was cut into a disk with a diameter of 10 mm from the sheet and dried at 353 K. A lithium-ion battery cell was assembled using the cathode, Li foil with a dimeter of 1.5 mm as the anode, polyethylene film as the separator, and 1 mol dm^{-3} $LiPF_6$ dissolved in a mixed solution of 50 vol.% ethylene carbonate and 50 vol.% dimethyl carbonate as electrolyte (Fig. 2). The assembly process was carried out in an argon-filled glove box, where the concentrations of water and oxygen were controlled at less than 10 ppm. The assembled cell

was cycled between 3.0 and 4.2 V (*vs.* Li^+/Li) at 140 mA g^{-1} based on $LiCoO_2$ weight (1 C) using a battery charge–discharge system (HJ1001SD8, Hokuto Denko Corporation, Tokyo, Japan). The charge–discharge test was finished after the charging process, which corresponds to 50% as the average state of charge, for all the cathodes measured by LIBS. After the charge–discharge test, the cathode was washed in a mixed solution of 50 vol.% ethylene carbonate and 50 vol.% dimethyl carbonate. Elemental mappings of the cathode were also collected using an SEM (S-3400 N, Hitachi High-Technologies Co., Tokyo, Japan) equipped with a lithium-drifted silicon (Si (Li)) EDX detector (EDAX Inc., New Jersey, USA).

XAS measurements of the cathode were performed by collecting spectra near the Co K-edge (7690–7750 eV) with an energy step of 0.35 eV at the BL-7C and BL-9C beamlines of Photon Factory (High Energy Accelerator Research Organization, Japan). The beam size of the X-ray was set to 500×500 μm in the x-y direction using a slit. The intensities of the incident and transmitted X-rays were measured using ion chambers. The analyzed positions of the cathode in the x and y directions were controlled with linear transition automatic stages. The chemical states of cobalt in $LiCoO_2$ were evaluated from the peak top energy of the XAS spectra under the assumption that the peak top energy linearly increased with a decrease in the proportion of Co(III) [12]. Cathodes before the charge–discharge test and after charging to 4.2 V at 14 mA g^{-1} based on $LiCoO_2$ weight (0.1 C) were used as references for the Co(III) state and the state of 50% Co(III) and 50% Co(IV), respectively. Typical spectra of the references are shown in Fig. S1.

3. Results and discussion

3.1 Calibration of LIBS measurement for lithium concentration

Determination of the lithium concentration in the cathode material of a lithium-ion battery cell requires a calibration curve obtained by performing LIBS measurements of

standard samples consisting of the cathode material. In the present study, we selected pressed pellets containing $LiCoO_2$ as the standard samples. Fig. 3 shows the emission spectra of a standard sample whose atomic ratio of lithium to cobalt was 0.80 (X = 0.80) in air and under an argon atmosphere of 1000 Pa. Two intense lithium emission lines at 610.4 and 670.8 nm were detected in the spectra. The lithium emission lines at 610.4 (Li I 610.4 nm line) and 670.8 nm (Li I 670.8 nm line) were attributed to the non-resonance transition (3.879 eV → 1.848 eV, $1s^2 3d \rightarrow 1s^2 2p$) and the resonance transition (1.848 eV → 0.000 eV, $1s^2 2p \rightarrow 1s^2 2s$), respectively. The intensities of these lines increased and their relative standard deviations decreased by replacing air with an argon atmosphere of 1000 Pa, as listed in Table 1. The densities of lithium atoms, including the ground state and excited states, in the plasma generated in an argon atmosphere of 1000 Pa are lower than those in air because the reduced pressure and argon gas expand the plasma [36]. The lower densities of lithium atoms in the plasma weaken the self-absorption effect, that is, the reabsorption of the emitted luminescence by the lithium atoms in the plasma. In addition, the number of excited lithium atoms, such as the states of $1s^2 3d$ and $1s^2 2p$, generated in an argon atmosphere of 1000 Pa is larger than that in air because argon gas enhances the plasma temperature [36]. For these reasons, the Li I 610.4 nm and Li I 670.8 nm lines increased and their relative standard deviations decreased by replacing air with an argon atmosphere of 1000 Pa. However, the intensities of the lithium emission line at 670.8 nm were constant at higher lithium concentrations, such as for the standard samples with X = 0.51, 0.62, and 0.80, as shown in Table 1 and Supplementary Fig. S2, which arose from the self-absorption. Their standard deviations were relatively high. However, the intensities of the Li I 610.4 nm line increased with increasing lithium concentration, and their standard deviations were relatively low. These results indicated that the Li I 670.8 nm line was affected by the self-absorption more strongly than the Li I 610.4 nm line. Lithium atoms in the ground state ($1s^2 2s$) and an excited state of $1s^2 2p$ are

responsible for the self-absorption of the Li I 610.4 nm and Li I 670.8 nm lines, respectively. The number of lithium atoms in the ground state is expected to be approximately more than one order of magnitude greater than that in the excited state of $1s^2 2p$ from a rough estimation using Boltzmann distribution of the two states under the assumption that the temperature of the plasma was 10000 K [38]. Therefore, the self-absorption effect of the Li I 670.8 nm line was stronger than that of the Li I 610.4 nm line. The greater relative standard deviation of the Li I 670.8 nm line also arose from its stronger self-absorption effect. It was, therefore, concluded from the present results that the Li I 610.4 nm line was suitable for quantitative analysis of lithium because of its lower self-absorption effect and lower relative standard deviations. We found that the intensities of the lithium emission lines at 1000 Pa were the highest by changing the pressure in the sample chamber from 5 Pa to 1500 Pa. The obtained calibration curve of the Li I 610.4 nm line in an argon atmosphere of 1000 Pa is shown in Fig. 4. We used the calibration curve for the quantitative analysis of lithium in the following study. It should be noted that the Li I 610.4 nm line was still somewhat affected by self-absorption because the calibration curve negatively deviated from a straight line.

3.2 Lithium mapping of the cathode

The self-absorption effect was reduced by performing LIBS measurements in a reduced argon atmosphere. As a result, the linearity between the emission intensity of the Li I 610.4 nm line and lithium concentration was improved at higher lithium concentrations when compared with that measured in an ambient air atmosphere. Then, we attempted to obtain quantitative lithium mapping of the cathodes of a lithium-ion battery using the calibration curve obtained in an argon atmosphere of 1000 Pa (Fig. 4). In the LIBS mapping measurement, we measured the emission intensities of the quarter circle area of the cathodes. The pitch of the measured point on the cathodes was 300 μm because the diameter of the hole formed by the irradiation of the single pulse laser was 250 μm.

Fig. 5 (a) and (b) shows the lithium mapping of the cathodes cycled 30 and 50 times, respectively, obtained by LIBS measurement. The atomic ratio of lithium to cobalt was calculated with the assumption that the emission intensity of the cathode before the charge–discharge test corresponded to that of $LiCoO_2$ (X = 1.0). We were unable to obtain the lithium mapping of the right half of the cathode cycled 50 times because the cathode was torn as we removed it from the cell after the charge–discharge test. The mappings represent the average lithium ratio within the depth of 50 ± 10 μm from their surfaces. The depth was measured by observing dimples formed after the irradiation of the single pulse laser using a digital microscope (VHX-1000, KEYENCE Corp., Osaka, Japan). The lithium distribution of the cathode cycled 30 times was relatively homogeneous, while that cycled 50 times was inhomogeneous: the lithium ratio was high around the edge and low near the center. The atomic ratios of lithium to cobalt were higher than 1.0 at four points around the edge of the cathode cycled 50 times, as shown by the red dots in Fig. 5 (b). We also detected a large area with $X > 1.0$ in another cathode cycled 50 times, as shown in Fig. 5 (c). These results implied that lithium compounds other than $LiCoO_2$ may be precipitated on the cathodes cycled 50 times. Subsequently, we obtained EDX elemental mappings of another area of the cathode, shown in Fig. 5 (c), to identify the compounds. We found that the intensities of the F and P K lines around the edge of the cathode were higher than those near the center, as shown in Fig. 6 (b) and (c). These results suggested that LiF and PF_5, which are decomposition products of $LiPF_6$, precipitated and coated on the edge of the cathode, as has previously been reported [39-41]. In addition, the intensity of the Co K line around the edge of the cathode were slightly lower than that near the center, as shown in Fig. 6 (d). This indicated that the cathode around the edge was overcharged and that $LiCoO_2$ in the area dissolved into the electrolyte, as has previously been reported [42]. Comparing Fig. 5 (a), (b), and (c), LiF and PF_5 were formed from the edge to the center of the cathode. This could be because the amount of the

electrolyte contacted with the edge of the cathode was much larger than that with the center, as shown in Fig. 2. It is also speculated that the millimeter scale distribution of LiF and PF_5 might be related to the overcharge and subsequent temperature rise at the edge of the cathode. The overcharge and temperature rise might lead to the decomposition of the electrolyte, the precipitation of $LiPF_6$, and the subsequent spontaneous decomposition of $LiPF_6$. Therefore, we can detect a symptom of precipitating LiF on a cathode by detecting an area with $X > 1.0$ by LIBS.

XAS measurements were performed on cathodes cycled 10 and 50 times and the obtained chemical state mappings of cobalt for the cathode are shown in Fig. 7 (a) and (b), respectively. The pitch of the measured points on the cathodes was 500 μm. The Co(III) distribution of the cathode cycled 10 times was homogeneous, while that cycled 50 times was inhomogeneous: the ratios of Co(III) were high near the center and at a few points around the edge. We also obtained the lithium mapping of the cathodes by performing LIBS measurements for the same areas measured by XAS, as shown in Fig. 7 (d) and (e). The distribution tendency of lithium for both the cathodes were relatively similar to that of Co(III). It is reasonable that the chemical state was Co(III) in the area where LiF was detected, because the decomposition of the electrolyte demands electrons [39] and LiF is thus formed during the reduction reaction. These results indicated that the lithium mappings of the cathodes measured by LIBS represented their reaction distributions to some extent because the distribution of the chemical state of cobalt exhibits the reaction distribution of $LiCoO_2$ [4,12]. However, it should be noted that the precision of lithium ratios measured by LIBS was not as good as that of the Co(III) ratios measured by XAS. This may be because the cathodes were porous, which led to the increase of the standard deviation of the emission intensities of lithium.

The spatial resolution of LIBS measurements in the present study was approximately 250 μm in plane and 50 μm in depth, which was not sufficient for investigating the reaction distribution of a cathode of a lithium-ion battery. This is because the pulse duration of the laser in our LIBS measurement was 16–18 ns. We can achieve a spatial resolution in the sub-micrometer range in plane and nanometer range in depth by using a laser with a femtosecond pulse duration [10,25-29]. This spatial resolution would then be sufficient for investigating the reaction distribution of the cathode.

4. Conclusions

We have demonstrated that we can quantitatively acquire the lithium distribution of a cathode material, consisting of $LiCoO_2$, acetylene black, and polytetrafluoroethylene, of a lithium-ion battery by performing LIBS measurements in an argon atmosphere of 1000 Pa. We used a calibration curve obtained by measuring the emission intensities at 610.4 nm of the standard samples, whose composition ratios of lithium to cobalt were 0, 0.10, 0.30, 0.51, 0.62, 0.80, and 0.99. When we performed the LIBS measurements for cathodes cycled 10 and 50 times between 3.0 and 4.2 V (*vs.* Li^+/Li) at 140 mA g^{-1} based on $LiCoO_2$ weight (1 C), the lithium distributions of the cathodes were somewhat similar to the distribution of Co(III) acquired by XAS measurement, which can quantitatively exhibit their reaction distribution. Additionally, it is possible to detect a symptom of precipitating decomposition products of the electrolyte, LiF, on the cathode from the lithium distributions of the cathode measured by LIBS. Although it is difficult to obtain the lithium distribution of a cathode of a lithium-ion battery *in situ* and the precision of the lithium ratios were not as good as that of the Co(III) ratios measured by XAS, LIBS can provide a relatively quantitative lithium distribution of the cathode by laboratory-scale measurements, which is an advantage over XAS measurements.

Acknowledgements

Financial support for the present study was provided by JSPS KAKENHI Grant Number 16K14444. The X-ray absorption spectroscopy measurements were performed under the approval of the Photon Factory Program Advisory Committee (Proposal No. 2017G144 and 2015G634).

References

[1] H. Liang, X. Qiu, H. Chen, Z. He, W. Zhu, L. Chen, Electrochem. Commun. 6 (2004) 789–794.

[2] S. Huang, Z. Wen, X. Yang, Z. Gu, X. Xu, J. Power Sources 148 (2005) 72–77.

[3] M. Okubo, E. Hosono, J. Kim, M. Enomoto, N. Kojima, T. Kudo, H. Zhou, I. Honma, J. Am. Chem. Soc. 129 (2007) 7444–7452.

[4] T. Nakamura, T. Watanabe, K. Amezawa, H. Tanida, K. Ohara, Y. Uchimoto, Z. Ogumi, Solid State Ion. 262 (2014) 66–69.

[5] J. Liu, M. Kunz, K. Chen, N. Tamura, T.J. Richardson, J. Phys. Chem. Lett. 1 (2010) 2120–2123.

[6] G. Ouvrard, M. Zerrouki, P. Soudan, B. Lestriez, C. Masquelier, M. Morcrette, S. Hamelet, S. Belin, A.M. Flank, F. Baudelet, J. Power Sources 229 (2013) 16–21.

[7] W.C. Chueh, F.E. Gabaly, J.D. Sugar, N.C. Bartelt, A.H. McDaniel, K.R. Fenton, K.R. Zavadil, T. Tyliszczak, W. Lai, K.F. McCarty, Nano Lett. 13 (2013) 866–872.

[8] M. Katayama, K. Sumiwaka, R. Miyahara, H. Yamashige, H. Arai, Y. Uchimoto, T. Ohta, Y. Inada, Z. Ogumi, J. Power Sources 269 (2014) 994–999.

[9] H. Tanida, H. Yamashige, Y. Orikasa, Y. Gogyo, H. Arai, Y. Uchimoto, Z. Ogumi, J. Phys. Chem. C 120 (2016) 4739–4743.

[10] P. Smyrek, J. Pröll, H.J. Seifert, W. Pfleging, J. Electrochem. Soc. 163 (2016) A19–A26.

[11] T. Uenoyama, R. Miyahara, M. Katayama, Y. Inada, J. Phys. Conf. Ser. 712 (2016) 012143.

[12] T. Nakamura, T. Watanabe, Y. Kimura, K. Amezawa, K. Nitta, H. Tanida, K. Ohara, Y. Uchimoto, Z. Ogumi, J. Phys. Chem. C 121 (2017) 2118–2124.

[13] M. Kerlau, M. Marcinek, V. Strinivasan, R.M. Kostecki, Electrochim. Acta 52 (2007) 5422–5429.

[14] J. Nanda, J. Remillard, A. O'Neill, D. Bernardi, T. Ro, K.E. Nietering, J-Y. Go, T.J. Miller, Adv. Funct. Mater. 21 (2011) 3282–3290.

[15] F. Meirer, J. Cabana, Y. Liu, A. Mehta, J.C. Andrews, P. Pianetta, J. Synchrotron Rad. 18 (2011) 773–781.

[16] R. Robbert, D. Zeng, A. Lanzirotti, P. Adamson, S.J. Clarke, C.P. Grey, Chem. Mater. 24 (2012) 2684–2691.

[17] J. Zhou, J. Wang, Y. Hu, T. Regier, H. Wang, Y. Yang, Y. Cui, H. Dai, Chem. Commun. 49 (2013) 1765–1767.

[18] F. Yang, Y. Liu, S.K. Martha, Z. Wu, J.C. Andrews, G.E. Ice, P. Pianetta, J. Manda, Nano Lett. 14 (2014) 4334–4341.

[19] J. Wang, Y.K. Chen-Wiegart, J. Wang, Nature Comm. 5 (2014) 4570.

[20] D.C. Bock, R.V. Tappero, K.J. Takeuchi, A.C. Marschilok, E.S. Takeuchi, ACS Appl. Mater. Interfaces 7 (2015) 5429–5437.

[21] L. Nowack, D. Grolimund, V. Samson, F. Marone, V. Wood, Sci. Rep. 6 (2016) 21479.

[22] Y. Orikasa, Y. Gogyo, H. Yamashige, M. Katayama, K. Chen, T. Mori, K. Yamamoto, T. Masese, Y. Inada, T. Ohta, Z. Siroma, S. Kato, H. Kinoshita, H. Arai, Z. Ogumi, Y. Uchimoto, Sci. Rep. 6 (2016) 26382.

[23] R.E. Ruther, A.S. Pandian, P. Yan, J.N. Weker, C. Wang, J. Nanda, Chem. Mater. 29 (2017) 2997–3005.

[24] F.C. Strobridge, B. Orvananos, M. Croft, H-C. Yu, R. Robert, H. Liu, Z. Zhong, T. Connolley, M. Darkopoulos, K. Thornton, C.P. Grey, Chem. Mater. 27 (2015) 2374–2386.

[25] V. Zorba, J. Syzdek, X. Mao, R.E. Russo, R. Kostecki, App. Phys. Lett. 100 (2012) 234101.

[26] L. Cheng, E.J. Crumlin, W. Chen, R. Qiao, H. Hou, S.F. Lux, V. Zorba, R. Russo, R. Kostecki, Z. Liu, K. Persson, W. Yang, J. Cabana, T. Richardson, G. Chen, M. Doeff, Phys. Chem. Chem. Phys. 16 (2014) 18294–18300.

[27] L. Cheng, J.S. Park, H. Hou, V. Zorba, G. Chen, T. Richardson, J. Cabana, R. Russo, M. Doeff, J. Mater. Chem. A 2 (2014) 172–181.

[28] H. Hou, L. Cheng, T. Ichardson, G. Chen, M. Doeff, R. Zheng, R. Russo, V. Zorba, J. Anal. Spectrom. 30 (2015) 2295–2302.

[29] P. Gotcu, W. Pfleging, P. Smyrek, H.J. Seifert, Phys. Chem. Chem. Phys. 19 (2017) 11920–11930.

[30] M. Ebner, F. Marone, M. Stampanoni, V. Wood, Science 342 (2013) 716–720.

[31] N. Balke, S. Jesse, A.N. Morozovska, E. Eliseev, D.W. Chung, Y. Kim, L. Adamczyk, R.E. García, N. Dudney, S.V. Kalnin, Nature Nanotechnol. 5 (2010) 749–754.

[32] K, Mima, R. Gonzalez-Arrabal, H. Azuma, A. Yamazaki, C. Okuda, Y. Ukyo, H. Sawada, K. Fujita, Y. Kato, J.M. Perlado, S. Nakai, Nucl. Instrum. Methods Phys. Res. Sect. B-Beam Interact. Mater. Atoms 290 (2012) 79–84.

[33] X. Zhang, T.W. Verhallen, F. Labohm, M. Wagemaker, Adv. Energy Mater. 5 (2015) 1500498.

[34] D. Robert, T. Douillard, A. Boulineau, G. Brunetti, P. Nowakowski, D. Vanet, P. Bayle-Guillemaund, C. Cayron, ACS Nano 7 (2012) 10887–10894.

[35] C. Fabre, M-C. Boiron, J. Dubessy, A. Chabriron, B. Charoy, T.M. Crespo, Geochim. Cosmochim. Acta 66 (2002) 1401–1407.

[36] R. Noll, Laser-Induced Breakdown Spectrometry Fundamentals and Applications, Springer, Heidelberg, 2012, pp.29–33.

[37] L. Peter, R. Noll, Appl. Phys. B 86 (2007) 159–167.

[38] T. A. Labutin, A. M. Popov, V. N. Lednev, N. B. Zorov, Spectrochim. Acta Part B 64 (2009) 938–949.

[39] Y. Wang, X. Guo, S. Greenbaum, J. Liu, K. Amine, Electrochem. Solid State Lett. 4 (2001) A68–A70.

[40] D. Ostrovskii, F. Ronci, B. Scrosati, P. Jacobsson, J. Power Sources 94 (2001) 183–188.

[41] M. Balasubramanian, H.S. Lee, X. Sun, X.Q. Yang, A.R. Moodenbaugh, J. McBreen, D.A. Fischer, Z. Fu, Electrochem. Solid State Lett. 5 (2002) A22–A25.

[42] G.G. Amatucci, J.M. Trascon, L.C. Klein, Solid State Ion. 83 (1996) 167–173.

Figure captions

Figure 1. Schematic illustration of the LIBS system.

Figure 2. Schematic illustration of the assembled lithium-ion battery cell.

Figure 3. LIBS spectra of the standard sample with $X = 0.80$ (a) in air and (b) 1000 Pa argon. The spectra were obtained using the Echelle-type spectrograph.

Figure 4. Calibration curve of the Li I 610.4 nm line measured in 1000 Pa argon. The measurements were carried out more than 10 times for each standard sample. The data were obtained using the Czerny-Turner spectrograph.

Figure 5. LIBS mappings of atomic ratios of lithium to cobalt (X) for the cathode cycled (a) 30 times, (b) 50 times, and (c) another 50 times. The blue dots represent the unmeasured area.

Figure 6. (a) SEM image and EDX elemental mappings of (b) F, (c) P, and (d) Co for the cathode shown in Fig. (c).

Figure 7. XAS chemical state mappings of cobalt for the cathode cycled (a) 10 times and (b) 50 times. The corresponding LIBS mappings of atomic ratios of lithium to cobalt (X) for the cathode cycled (c) 10 times and (d) 50 times. The blue dots represent the unmeasured area.

Figure S1. Co K-edge XAS spectra of reference cathodes of the Co(III) state and the state of 50% Co(III) and 50% Co(IV).

Figure S2. Calibration curve of the Li I 610.4 nm and Li I 670.6 nm lines measured in air and 1000 Pa argon. The measurements were carried out more than 10 times for each standard sample. The data were obtained using the Echelle-type spectrograph.

Table 1 Intensities and relative standard deviation (RSD) of the standard samples for the Li I 610.4 nm and Li I 670.6 nm lines measured in air and 1000 Pa argon. The measurements were carried out more than 10 times for each standard sample. The data were obtained using the Echelle-type spectrograph.

Atmosphere	Air				Argon (1000 Pa)			
Emission line	610.4 nm		670.6 nm		610.4 nm		670.6 nm	
Composition ratio of Li / Co (X)	Intensity [a.u.]	RSD [%]	Intensity [a.u.]	RSD [%]	Intensity [a.u.]	RSD [%]	Intensity [a.u.]	RSD [%]
0.10	14135	6.9	6385	17.1	27023	7.0	59359	5.2
0.30	19558	15.0	4982	32.5	42750	4.2	71597	4.5
0.51	24554	11.1	9480	26.3	51740	3.9	81618	8.3
0.62	29781	10.4	7911	27.6	68352	1.7	83241	9.7
0.80	30438	7.0	8668	17.0	75799	3.6	84408	8.3

Figure 1.

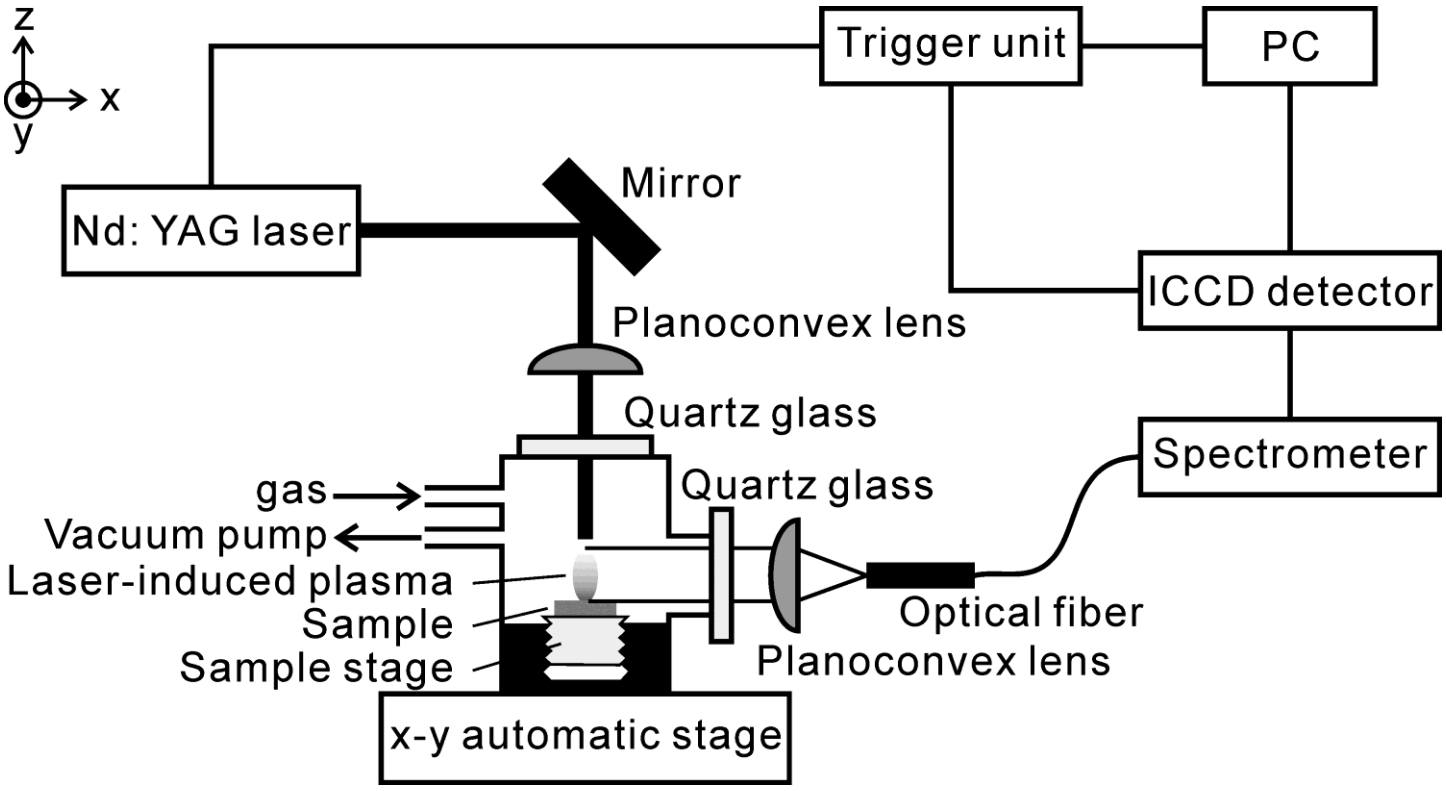
z
x
y
Trigger unit
PC
Nd: YAG laser
Mirror
ICCD detector
Planoconvex lens
Quartz glass
Spectrometer
gas
Quartz glass
Vacuum pump
Laser-induced plasma
Sample
Optical fiber
Sample stage
Planoconvex lens
x-y automatic stage

Figure 2.

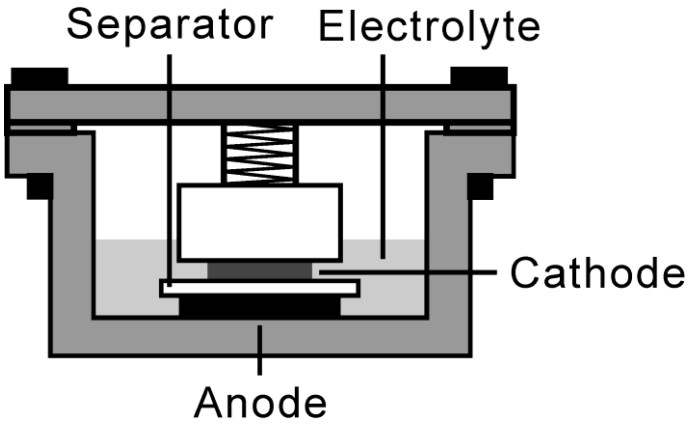

Figure 3.

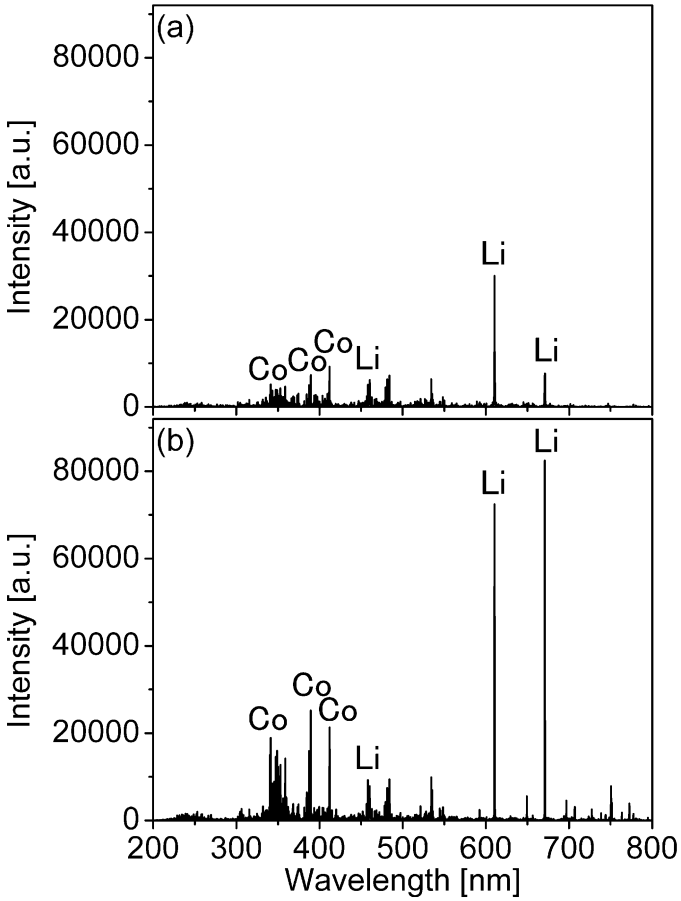

Figure 4.

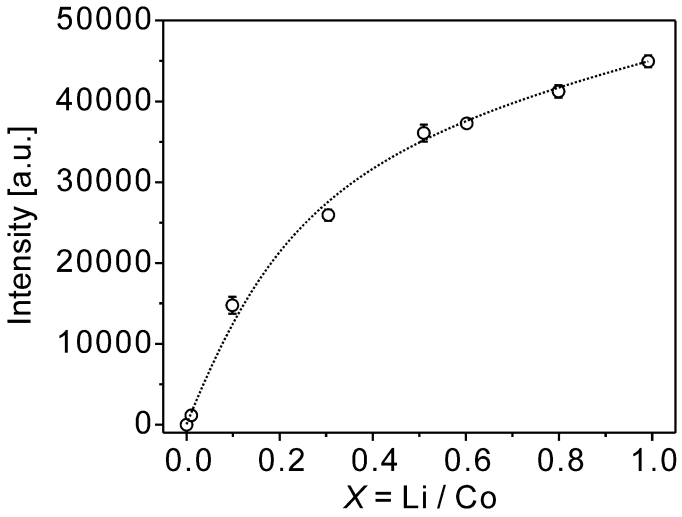
50000
40000
30000
20000
10000
0
Intensity [a.u.]
0.0
0.2
0.4
0.6
0.8
1.0
X = Li / Co

Figure 5.

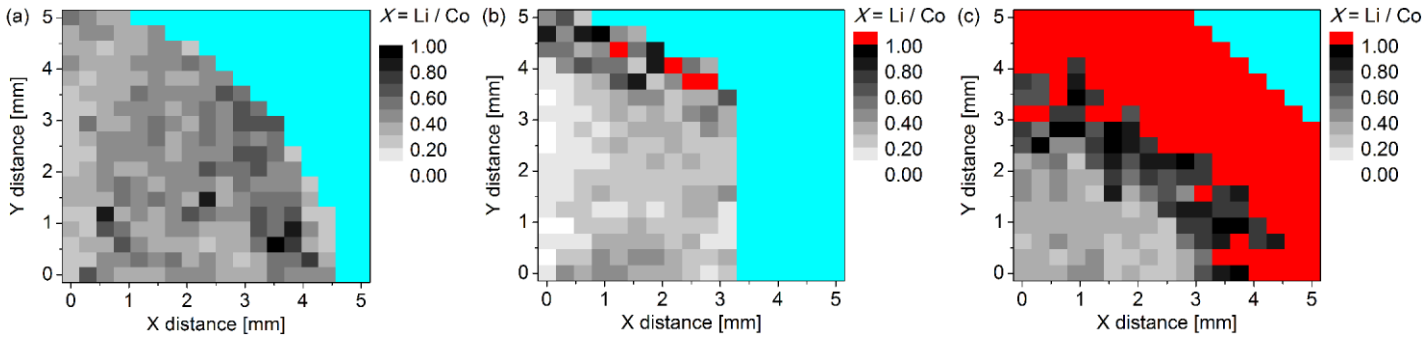

Figure 6.

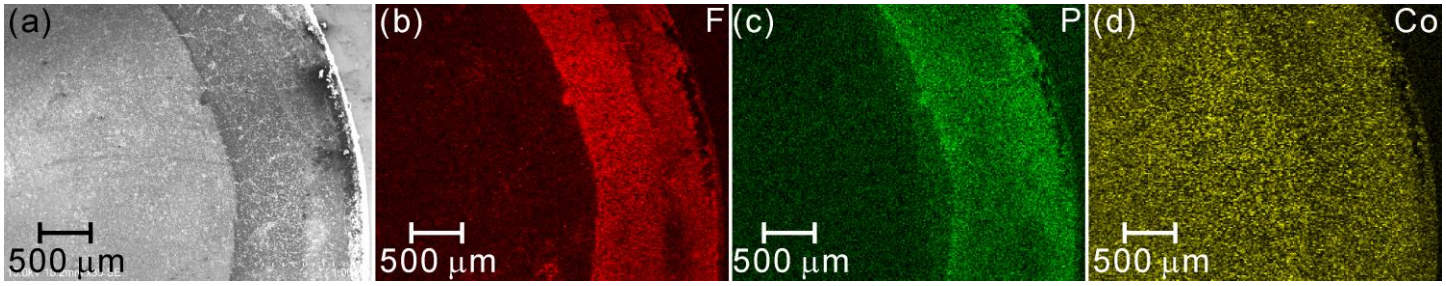

Figure 7.

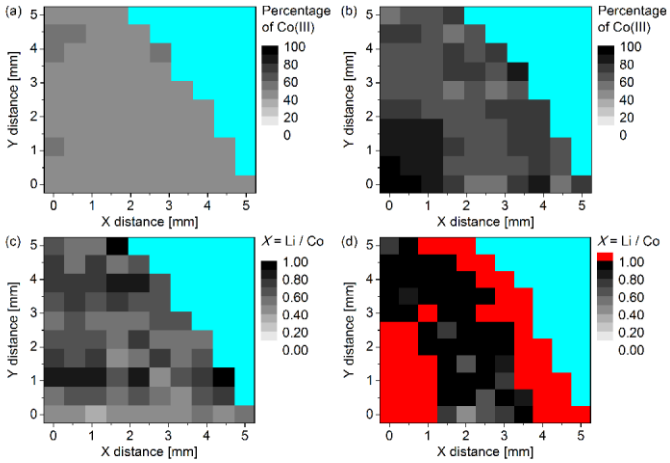
(a)
(b)
(c)
(d)
Percentage of Co(III)
100
80
60
40
20
0
X = Li / Co
1.00
0.80
0.60
0.40
0.20
0.00
Y distance [mm]
X distance [mm]

Figure S1.

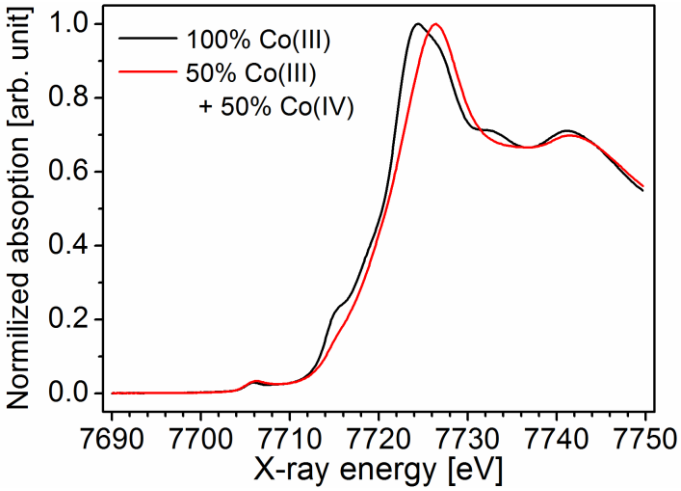
100% Co(III)
50% Co(III)
+ 50% Co(IV)
Normilized absoption [arb. unit]
1.0
0.8
0.6
0.4
0.2
0.0
7690
7700
7710
7720
7730
7740
7750
X-ray energy [eV]

Figure S2.

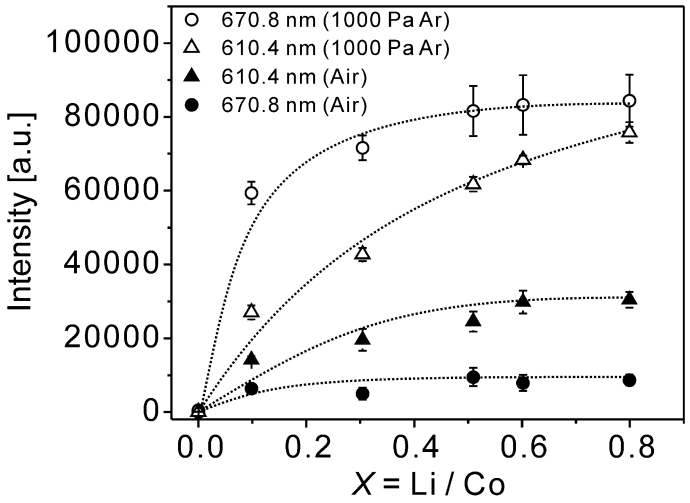
670.8 nm (1000 Pa Ar)
610.4 nm (1000 Pa Ar)
610.4 nm (Air)
670.8 nm (Air)
Intensity [a.u.]
100000
80000
60000
40000
20000
0
0.0
0.2
0.4
0.6
0.8
X = Li / Co